NASA TECHNICAL NOTE

NASA TN D-6947

ANALYTICAL DESIGN OF SENSORS FOR MEASURING ATMOSPHERIC TEMPERATURE DURING TERMINAL PHASE OF PLANETARY ENTRY

by John P. Millard, Michael J. Green, and Simon C. Sommer

Ames Research Center
Moffett Field, Calif. 94035

NATIONAL AERONAUTICS AND SPACE ADMINISTRATION • WASHINGTON, D. C. • AUGUST 1972

1. Report No.	2. Government Accession No.	3. Recipient's Catalog No.
NASA TN D-6947		

4. Title and Subtitle	5. Report Date
ANALYTICAL DESIGN OF SENSORS FOR MEASURING ATMOSPHERIC TEMPERATURE DURING TERMINAL PHASE OF PLANETARY ENTRY	August 1972
	6. Performing Organization Code

7. Author(s)	8. Performing Organization Report No.
John P. Millard, Michael J. Green, and Simon C. Sommer	A-4412
	10. Work Unit No. 117-07-04-14
9. Performing Organization Name and Address	11. Contract or Grant No.
NASA Ames Research Center Moffett Field, California 94035	
	13. Type of Report and Period Covered
12. Sponsoring Agency Name and Address	Technical Note
National Aeronautics and Space Administration Washington, D. C., 20546	14. Sponsoring Agency Code

15. Supplementary Notes

16. Abstract

An analytical study was conducted to develop a sensor for measuring the temperature of a planetary atmosphere from an entry vehicle traveling at supersonic speeds and having a detached shock. Such a sensor has been used in the Planetary Atmosphere Experiments Test Probe (PAET) mission and is planned for the Viking-Mars mission. The study specifically considered butt-welded thermocouple sensors stretched between two support posts; however, the factors considered are sufficiently general to apply to other sensors as well. This study included: (1) an investigation of the relation between sensor-measured temperature and free-stream conditions; (2) an evaluation of the effects of extraneous sources of heat; (3) the development of a computer program for evaluating sensor response during entry; and (4) a parametric study of sensor design characteristics.

The results of the parametric study show that inaccurate knowledge of the recovery temperature ratio is the potential source of the greatest error for the sensor designed for the PAET-Earth mission with deployment at Mach number 2. The effects of radiation are negligible for this particular mission. For deployment at Mach number 3, the sensor does not track recovery temperature as well because the temperatures are high and changing rapidly with time. If the sensor wire designed for PAET were shortened by a factor of 2, errors induced by conduction effects would increase by about 2° K. However, if this short sensor were used for the Viking-Mars mission, errors of the order of 50° K would result. Thus, it cannot be assumed that a sensor designed for one mission will be adequate for another.

17. Key Words (Suggested by Author(s))	18. Distribution Statement
Atmospheric temperature sensor Convective heat transfer Planetary atmosphere experiments Test Probe (PAET) Viking-Mars Thermocouples	Unclassified – Unlimited

19. Security Classif. (of this report)	20. Security Classif. (of this page)	21. No. of Pages	22. Price*
Unclassified	Unclassified	27	$3.00

* For sale by the National Technical Information Service, Springfield, Virginia 22151

NOMENCLATURE

a	speed of sound, m/sec
A	cross-sectional area of sensor wire, m^2
c_p	specific heat, J/kg °K
C	circumference of sensor wire, m
C_p	pressure coefficient, $\frac{p_L - p_\infty}{q_\infty}$, dimensionless
D	diameter of sensor wire, m
F_p	view factor for planetary radiation, dimensionless
F_S	view factor for solar radiation, dimensionless
F_V	view factor for vehicle-emitted radiation, dimensionless
h_c	convective heat-transfer coefficient, W/m^2 °K
k	thermal conductivity, W/m °K
L	length of sensor wire, m
m	parameter defined by equation (15), per m
M	Mach number, $\frac{V}{a}$, dimensionless
Nu	Nusselt number, $\frac{h_c D}{k_a}$, dimensionless
p	pressure, N/m^2
q	dynamic pressure, $\frac{\rho V^2}{2}$, N/m^2
Q	heat-transfer rate, W/m^2
R	gas constant for a particular gas, J/kg °K
Re	Reynolds number, $\frac{\rho V D}{\mu}$, dimensionless
RTR	recovery temperature ratio, $\frac{T_R}{T_t}$, dimensionless
S	solar constant, W/m^2

$\frac{S}{R_B}$	ratio of length measured along forebody surface, from axis of vehicle, to maximum radius of forebody
t	time, sec
T	temperature, °K
V	speed, m/sec
x	distance along sensor wire, m
α	absorptance of sensor wire for radiation emitted by a particular source, dimensionless
γ	ratio of specific heats, $\frac{c_p}{c_v}$, dimensionless
ϵ	emittance of a particular source of radiant energy, dimensionless
μ	dynamic viscosity, N sec/m^2
ρ	density, kg/m^3
σ	Stefan-Boltzmann constant, W/m^2 °K^4
τ	time constant, sec

Subscripts and Special Notation

a	atmosphere
c	convection
L	local
p	planet
R	recovery
s	sensor
S	Sun
t	total
v	vehicle

(x,t)	location x on sensor wire at time t
∞	free stream

ANALYTICAL DESIGN OF SENSORS FOR MEASURING ATMOSPHERIC TEMPERATURE DURING TERMINAL PHASE OF PLANETARY ENTRY

John P. Millard, Michael J. Green, and Simon C. Sommer

Ames Research Center

SUMMARY

An analytical study was conducted to develop a sensor for measuring the temperature of a planetary atmosphere from an entry vehicle traveling at supersonic speeds and having a detached shock. Such a sensor has been used in the Planetary Atmosphere Experiments Test Probe (PAET) mission and is planned for the Viking-Mars mission. The study specifically considered butt-welded thermocouple sensors stretched between two support posts; however, the factors considered are sufficiently general to apply to other sensors as well. This study included: (1) an investigation of the relation between sensor-measured temperature and free-stream conditions; (2) an evaluation of the effects of the extraneous sources of heat; (3) the development of a computer program for evaluating sensor response during entry; and (4) a parametric study of sensor design characteristics.

The results of the parametric study show that inaccurate knowledge of the recovery temperature ratio is the potential source of the greatest error for the sensor designed for the PAET-Earth mission with deployment at Mach number 2. The effects of radiation are negligible for this particular mission. For deployment at Mach number 3, the sensor does not track recovery temperature as well because the temperatures are high and changing rapidly with time. If the sensor wire designed for PAET were shortened by a factor of 2, errors induced by conduction effects would increase by about 2° K. However, if this short sensor were used for the Viking-Mars mission, errors of the order of 50° K would result. Thus, it cannot be assumed that a sensor designed for one mission will be adequate for another.

INTRODUCTION

An atmospheric temperature sensor was selected as one of the instruments to be flown aboard the Planetary Atmosphere Experiments Test (PAET) vehicle. This vehicle was to enter the Earth's atmosphere at a velocity of 7000 m/sec with the mission of evaluating techniques for measuring atmospheric composition and structure. The temperature sensor was to provide a measurement of free-stream ambient temperature, as a function of altitude in the terminal phases of entry, to an accuracy of 10° K or better. The sensor was to be deployed when the vehicle had slowed, because of drag to about Mach number 2 or 3, after which it was to remain operational until impact. The sensor was positioned on the front face, near the base of the vehicle forebody, and extended beyond the boundary layer but behind the main shock wave.

The sensor selected was a butt-welded thermocouple stretched between two support posts. Its advantages are (1) the wire diameter can be specified to yield a tailormade time response for a specific mission (wires as small as 0.025-mm dia could be used), (2) the temperature at the butt-weld junction can be made independent of support-post temperature by the use of sufficiently long wires, (3) metals usually have a higher reflectance for solar and infrared radiation than do other materials, thus reducing solar and infrared inputs; and (4) the cylindrical configuration of a rolled butt-welded joint is a configuration for which there is much heat-transfer data in the literature.

An analytical study was undertaken as a basis for the design of a butt-welded thermocouple sensor that would yield reliable data. This study included: (1) an investigation of the relation between sensor-measured temperature and free-stream conditions; (2) an evaluation of the effects of extraneous sources of heat; (3) development of a computer program for evaluating sensor response during entry; and (4) a parametric study of sensor design characteristics.

This paper documents the analytical study and illustrates its value. The factors considered and the computer program used are sufficiently general to apply to similar missions. Numerical examples pertain to possible Earth or Mars missions; PAET was to be tested first in the Earth's atmosphere, and a similar temperature sensor is planned for the Viking-Mars mission.

FACTORS INFLUENCING MEASUREMENT

The measurement of free-stream ambient temperature with a sensor located behind a shock wave is a complex problem. The ambient temperature must be determined indirectly from a measurement of total temperature, which for reference is defined in equation (1) for a gas with constant ratio of specific heat γ. In the absence of radiation, total temperature is constant across a shock, and therefore the value at the sensor location is the same as in the free stream. Density and velocity vary with position behind a shock, however, and these influence sensor response time and efficiency of conversion of kinetic energy of the gas to thermal energy at the sensor. Thus, it is necessary to know the flow characteristics at the sensor location.

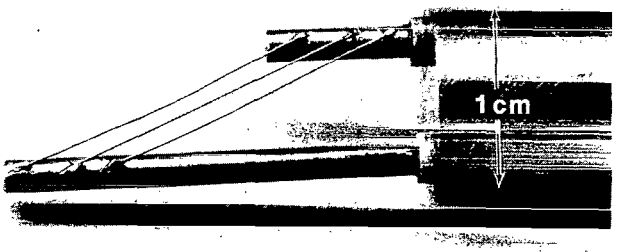

Figure 1. – Temperature sensor designed for PAET.

Another problem is that of extraneous heat sources, which can render a measurement meaningless: the Sun, planetary and vehicle infrared radiation, infrared emission of the sensor itself, and conduction through support leads. The importance of these heat sources can be evaluated only by comparing their heat inputs with that from the air stream, and their implications for sensor performance will vary with the particular mission.

In this section, factors that influence measurement are discussed in some detail

and incorporated into an energy equation for relating free-stream ambient temperature to sensor response. This discussion is general, but numerical values are presented that pertain to butt-welded thermocouple sensors and Earth and Mars missions. The sensor designed and constructed for PAET is shown in figure 1; the direction of flow is perpendicular to the plane of the page. For redundancy, this particular sensor contains three thermocouples mounted in parallel; for analysis, only one wire need be considered. Figure 2 illustrates the blunt-body PAET vehicle and its detached shock wave. This is a shadowgraph of a PAET model in a ballistic range at a Mach number of 3.[1] Tables 1 and 2 give trajectory and planetary data for the PAET and Mars missions.

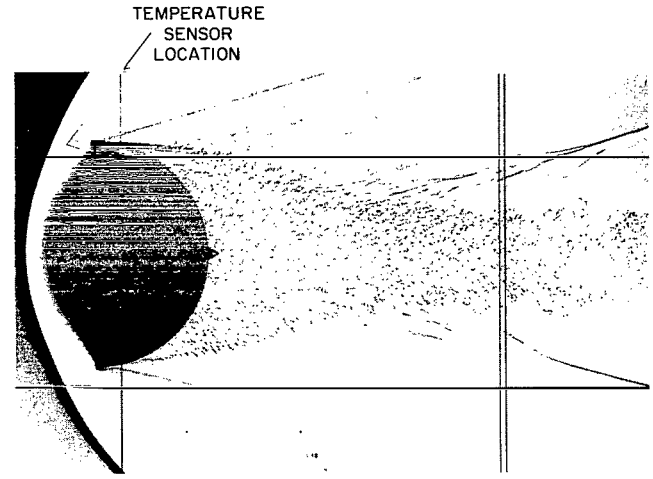

Figure 2. – Blunt-body PAET vehicle and detached shock wave.

Total Temperature

Total temperature is the measurement from which free-stream ambient temperature can be deduced. The relation is

$$T_t = T_\infty \left(1 + \frac{\gamma - 1}{2} M_\infty^{\,2}\right) \tag{1}$$

The term on the right is the sum of ambient temperature and the temperature increment contributed by kinetic energy of the gas molecules relative to the vehicle. An important consequence of this equation is that a vehicle undergoing rapid deceleration from high Mach numbers will encounter large and rapid changes in total temperature. This is illustrated in figure 3 for Earth and Mars missions. The measurement problem includes the accurate tracking of this rapidly varying total temperature (41° K/sec at $M = 2$ for PAET).

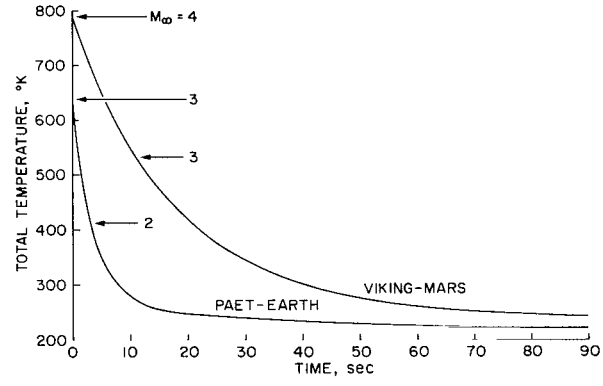

Figure 3. – Total temperature versus time for PAET and Viking missions.

In the design of the sensor, the free-stream ambient temperature profile and vehicle Mach number are assumed to be known; the total temperature versus time is

[1] Provided by courtesy of Mr. Robert I. Sammonds, Hypersonic Free Flight Branch, Ames Research Center, NASA.

computed from equation (1), and the response of a candidate sensor to that imposed temperature variation is sought.

Flow Conditions at Sensor Location

Values of Mach and Reynolds numbers at the location of the sensor influence the speed and efficiency of sensor response. In the following, variables necessary to evaluate these numbers are defined in terms of free-stream conditions. The definitions were obtained or deduced from reference 1.

Local Mach number can be written:

$$M_L = \left\{ \left[\left(1 + \frac{\gamma - 1}{2} M_\infty^2 \right) \left(\frac{p_{t,L}/p_{t,\infty}}{p_L/p_\infty} \right)^{\gamma - 1/\gamma} - 1 \right] \frac{2}{\gamma - 1} \right\}^{1/2} \tag{2}$$

where

$$\frac{p_L}{p_\infty} = 1 + C_p \left(\frac{\gamma}{2} \right) M_\infty^2 \tag{3}$$

For $M_\infty < 1$

$$\frac{p_{t,L}}{p_{t,\infty}} = 1 \tag{4}$$

and for $M_\infty \geq 1$

$$\frac{p_{t,L}}{p_{t,\infty}} = \left[\frac{(\gamma + 1) M_\infty^2}{(\gamma - 1) M_\infty^2 + 2} \right]^{\frac{\gamma}{\gamma - 1}} \left[\frac{\gamma + 1}{2\gamma M_\infty^2 - (\gamma - 1)} \right]^{\frac{1}{\gamma - 1}} \tag{5}$$

The ratio p_L/p_∞ depends on vehicle configuration and, for detached shock waves, is not easily or accurately computed. The work presented in this paper for the PAET mission is based upon experimental evaluations of the pressure coefficient C_p as defined by equation (3). Approximate values may be obtained from modified Newtonian theory: $C_p = C_{p_t} \cos^2 \theta$, where $C_{p_t} = [(p_{t,L}/p_\infty) - 1]/(q_\infty/p_\infty)$, and where θ is the angle between surface normal and vehicle axis.

Knowledge of local Mach number permits local temperature to be evaluated. The derivation follows from equation (1) and the constancy of total temperature in subsonic flow and across a shock

$$T_L = \frac{1 + \frac{\gamma - 1}{2} M_\infty^2}{1 + \frac{\gamma - 1}{2} M_L^2} T_\infty \tag{6}$$

Equations (2) and (6) can be used to evaluate local velocity and density:

$$V_L = M_L a_L = M_L \sqrt{\gamma R T_L} \tag{7}$$

$$\rho_L = \frac{p_L}{R T_L} \tag{8}$$

Conversion of Kinetic Energy at the Sensor

Total temperature has two components: the local ambient temperature and the contribution of local kinetic energy of the gas stream. Not all the kinetic energy is converted to heat at the sensor, and thus even under steady-state conditions a sensor will not record true total temperature. This incomplete conversion also implies that the effective temperature for driving a sensor is less than total temperature. The effective temperature for driving heat into a sensor—the temperature it attains when convective heat transfer goes to zero – is termed *recovery temperature.*

The magnitude of recovery temperature is influenced by sensor shape, size, orientation, Mach number, flow regime (continuum, slip, or free molecule), and, in some cases, the support-post configuration as it affects the flow of gas. Thus, for highest accuracy, a specific sensor should ultimately be evaluated in a wind tunnel under conditions representative of those in which it will be used. For design purposes, however, data reported in the literature can suffice. A good summary of data for cylindrical wires, which rolled butt-welded thermocouples approximate, is given by Baldwin et al. (ref. 2), who concluded that for transverse cylinders in continuum and slip flow, recovery temperature depends primarily on local Mach number and is almost entirely free of Reynolds number dependence for at least $30{,}000 > Re > 0.10$. This range is compatible with the Earth and Mars missions and possible sensors.

For reference, plots of the ratio of recovery temperature to total temperature

$$RTR = \frac{T_R}{T_t} \tag{9}$$

are given in figure 4 as a function of Mach number ($M \leq 1$). These data pertain to transverse cylinders in continuum slip flow; the data were summarized by Baldwin et al. (ref. 2) from refs. 3 and 4. The Mach number range 0 to 1 is presented here because the flow behind the PAET bow wave at the sensor location is subsonic.

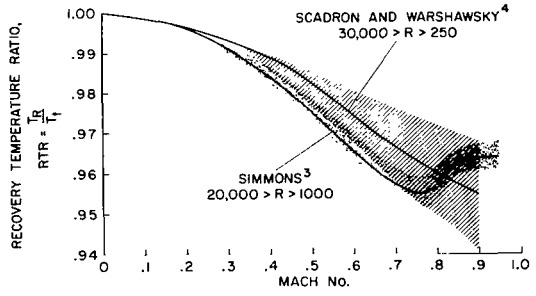

Figure 4. – Values of recovery temperature ratio versus Mach number reported in the literature for Reynolds numbers greater than 250 and for continuum flow.

Heat Transfer Rate to Sensor

The rate at which heat is transferred from an air stream to a sensor can be expressed by

$$Q_C = h_C(T_R - T_S)C\,dx \tag{10}$$

where h_C is the convective heat-transfer coefficient, $C\,dx$ is surface area of sensor, T_R is local recovery temperature, and T_S is sensor temperature. The convective heat-transfer coefficient is a function of sensor shape and size and local flow conditions. Its value is generally presented on a dimensionless plot of Nusselt number versus Reynolds number with Mach number as parameter for a specific sensor shape. The dimensionless plot of reference 2 for transverse cylinders is reproduced in figure 5.

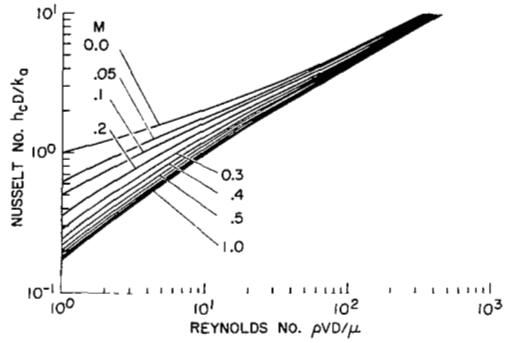

Figure 5. – Experimentally determined values of Nusselt number versus Reynolds number for transverse cylinders; curves are from reference 2.

The convective heat-transfer coefficient h_c directly influences speed of sensor response. The relation between time constant and h_c is

$$\tau = \frac{\rho c_p D}{4h_c} \tag{11}$$

where τ is the time in which a freely suspended sensor would respond by $1 - e^{-1}$, or 63.2 percent, to a step change in recovery temperature; ρ is sensor density; c_p is sensor specific heat; and D is sensor diameter.

Extraneous Heat Sources

A sensor of the type considered here cannot distinguish among the heating effects of different sources. Thus, the effects of solar heating are indistinguishable from those of convective heating caused by the gas stream. To ensure that a measurement pertains only to the air stream, effects of all other sources of heat should be evaluated to make certain they are negligible. Sources of heat can be categorized as: (1) radiant sources, which include the Sun, planet, and vehicle; (2) radiant self-emission of the sensor, and (3) conduction through support leads.

The solar heating effects on a sensor can be expressed

$$Q_S = \alpha_S F_S S C\, dx \tag{12}$$

where α_S is the absorptance of the sensor for sunlight, F_S is the view factor or effective portion of sensor exposed to the flux of one solar constant, S is the solar constant at the planet, and $C\,dx$ is surface area of the sensor. For a sensor exposed broadside to sunlight, F_S equals $1/\pi$; view factors are further described in reference 5. Analogously, the heating rates of a sensor due to planetary or vehicle infrared radiation are

$$Q_p = \alpha_p F_p \sigma T_p{}^4 C\, dx \tag{13}$$

and

$$Q_v = \alpha_v F_v \sigma T_v{}^4 C\, dx \tag{14}$$

where T_p and T_v are the temperatures of planet and vehicle. Sensor self-emission is defined as $\epsilon_s \sigma T_s{}^4 C\, dx$, where T_s is the temperature and ϵ_s is the emittance of the sensor.

Conduction effects are caused by the relatively massive support posts that do not rapidly track total temperature. Thus, heat is conducted from the center of the thermocouple wires to the support posts. As a first approximation, conduction effects may be made negligible by means of a formula for the steady-state temperature distribution in a wire anchored at both ends (ref. 6). This formula states that the temperature error at the center of the wire equals the difference between

recovery temperature and support-post temperature divided by cosh $m_L/2$, where L is the length of wire and m is defined by

$$m = \sqrt{h_c C/kA} \tag{15}$$

In this equation, h_c is the convective heat-transfer coefficient, C is the circumference of the wire, k is thermal conductivity of the wire, and A is the cross-sectional area of the wire. Equation (15) can be used in designing the wire sufficiently long to make the temperature error negligible.

ENERGY EQUATION AND COMPUTER SOLUTION

The factors that influence measurement were incorporated into an energy equation for relating free-stream ambient temperature to sensor response, and the equation was numerically solved by computer. To use the resulting computer program for design purposes, one would insert (1) vehicle trajectory data, (2) a probable atmospheric temperature profile and thermophysical data, and (3) details of sensor design into the program to determine sensor-measured temperature as a function of time. Any of the values can be altered to find the effect on sensor response.

Energy Equation

The energy equation pertains to a wire stretched between two support posts, and is a balance of heat terms on incremental lengths of wire dx as shown in figure 6. The equation considers (1) heat transferred from the air stream, (2) heat conducted along the wire, (3) absorbed sunlight, (4) absorbed infrared radiation from the planet, (5) absorbed infrared radiation from the entry vehicle, (6) sensor-emitted infrared radiation, and (7) changes in heat storage of the sensor. It can be written

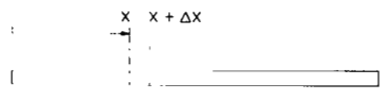

Figure 6. – Incremental length of wire on which energy balance is made

$$(\text{convection} + \text{conduction} + \text{solar} + \text{planet} + \text{vehicle})_{\text{input}} = \text{heat storage} + (\text{self emission} + \text{conduction})_{\text{output}}$$

That is,

$$h_c(T_R - T_S)C\,dx - kA\frac{\partial T_S}{\partial x} + (\alpha_S F_S S + \alpha_p F_p \sigma T_p{}^4 + \alpha_v F_v \sigma T_v{}^4)C\,dx = \rho c_p A\frac{\partial T_S}{\partial t}dx + \epsilon\sigma T_S{}^4 C\,dx - kA\left(\frac{\partial T_S}{\partial x} + \frac{\partial^2 T_S}{\partial x^2}dx\right) \tag{16}$$

where T_S is sensor temperature, and ρ, c_p, A, and C are sensor density, specific heat, cross-sectional area, and circumference, respectively. Recovery temperature, T_R, is defined by equation (9) and is obtained from a plot such as figure 4. The solar, planet, and vehicle radiation terms are defined in equations (12) through (14). The heat-transfer coefficient h_c is obtained from a dimensionless plot,

such as figure 5, of Nusselt number versus Reynolds number with Mach number as parameter. Equations (2) through (8) provide means of evaluating these dimensionless numbers. Viscosity or thermal conductivity are evaluated at total temperature where needed.

The sensor wire was subdivided into many incremental lengths dx (fig. 6), and the energy equation was solved for each length, but subject to defined boundary temperatures at the support posts.

Numerical Solution

For the numerical solution of the one-dimensional energy equation (16), we first rearrange the equation into the form

$$\frac{\partial T_S}{\partial t} + a(x)\frac{\partial^2 T_S}{\partial x^2} + b(x,t,T_S)T_S = c(t) \tag{17}$$

where

$$a(x) = \frac{k(x)}{\rho c_p} > 0$$

$$b(x,t,T_S) = \frac{C[h_C(t) + \epsilon\sigma T_S{}^3]}{\rho c_p A}$$

$$c(t) = \frac{C\{h_C(t)T_R(t) + \alpha_S F_S S + \alpha_p F_p \sigma[T_p(t)]^4 + \alpha_v F_v \sigma[T_v(t)]^4\}}{\rho c_p A}$$

and

$$T_S = T_S(x,t)$$

The parabolic partial differential equation (17) is quasilinear, since the coefficient b of the nonlinear term is not a function of the derivatives of the dependent variable T_S. The solution of this equation is uniquely determined in the semi-infinite strip R: $\{0 \le x \le L;\ t \ge 0\}$ by specifying the initial and boundary conditions:

$$\left.\begin{aligned} T_S(x,0) &= f(x) \qquad 0 \le x \le L \\ T_S(0,t) &= g_0(t) \qquad t > 0 \\ T_S(L,t) &= g_1(t) \qquad t > 0 \end{aligned}\right\} \tag{18}$$

The analytic solution of the initial boundary-value problem, equations (17) and (18), would specify T_S and its necessary derivatives as continuous functions of the two independent variables x and t. A set of mesh points $\{(x_j, t_n)$: $x_j = j(\Delta x)$ where $j = 0, 1, \ldots, J+1$ and $\Delta x = L/(J+1)$; $t_n = n(\Delta t)$, $n = 0, 1, \ldots\}$ is introduced on the strip R. The numerical solution is obtained by replacing the continuous variables by discrete variables at each mesh point (x_j, t_n).

The Crank-Nicholson finite-difference scheme is used in finding the numerical solution of equations (17) and (18). A description of this scheme, including restrictions for convergence and stability, and an error analysis, are given in reference 7. When the Crank-Nicholson procedure is applied, functions are evaluated at the point $(x_j,\ t_{n+1/2})$, which is halfway between the known temperature time level n and the unknown temperature time level $(n + 1)$. For subsequent notational convenience, let $\phi(x_j,\ t_n) = \phi_{j,\ n}$ and $T_s(x_j,\ t_n) = T_{j,\ n}$.

The Crank-Nicholson analogs to the continuous functions are

$$T_{j,n+1/2} \approx \frac{1}{2}\left(T_{j,n+1} + T_{j,n}\right) \tag{19}$$

$$\left(\frac{\partial T}{\partial t}\right)_{j,n+1/2} \approx \frac{1}{\Delta t}\left(T_{j,n+1} - T_{j,n}\right) \tag{20}$$

$$\left(\frac{\partial^2 T}{\partial x^2}\right)_{j,n+1/2} \approx \frac{1}{2(\Delta x)^2}\left[\left(T_{j+1,n+1} - 2T_{j,n+1} + T_{j-1,n+1}\right) + \left(T_{j+1,n} - 2T_{j,n} + T_{j-1,n}\right)\right] \tag{21}$$

Substituting equations (19) through (21) into equation (17) and rearranging transforms equation (17) for the time level (n + 1/2) into a system of algebraic equations

$$-u_j T_{j-1,n+1} + v_{j,n+1/2}\, T_{j,n+1} - u_j T_{j+1,n+1} = S_{j,n+1/2} \qquad 1 \le j \le J \tag{22}$$

where

$$u_j = \frac{\lambda}{2} a_j$$

$$\lambda = \frac{\Delta t}{(\Delta x)^2}$$

$$v_{j,n+1/2} = 1 + \lambda a_j + \frac{\Delta t}{2} b_{j,n+1/2}$$

and

$$S_{j,n+1/2} = u_j T_{j-1,n} + \left(2 - v_{j,n+1/2}\right)\ T_{j,n} + u_j T_{j+1,n} + (\Delta t) c_j$$

The boundary conditions given in equation (18) can be written as

$$\begin{aligned} T_{0,n+1} &= g_0(t_{n+1}) \\ T_{J+1,n+1} &= g_1(t_{n+1}) \end{aligned} \qquad n \ge 0 \tag{23}$$

Equations (22) and (23) form a system of equations in which the coefficient matrix is tridiagonal. The system is readily solved by using the line-inversion algorithm of reference 8, in which the quantities

$$d_j = \frac{u_j}{v_{j,n+1/2} - u_j d_{j-1}}$$

and

$$e_j = \frac{S^*_{j,n+1/2} + u_j e_{j-1}}{v_{j,n+1/2} - u_j d_{j-1}} \qquad j = 1, 2, \ldots, J$$

are computed, where $d_0 = e_0 = 0$;

$$S^*_{1,n+1/2} = S_{1,n+1/2} + u_1 T_{0,n+1}, S^*_{j,n+1/2} = S_{j,n+1/2} \qquad j = 2, 3, \ldots, J$$

and

$$S^*_{J,n+1/2} = S_{J,n+1/2} + u_J T_{J+1,n+1}$$

The temperature solution for the time level (n + 1) is obtained by backward substitution formulas:

$$T_{J,n+1} = e_j$$

$$T_{j,n+1} = d_j T_{j+1,n+1} + e_j \qquad j = J-1, J-2, \ldots, 1$$

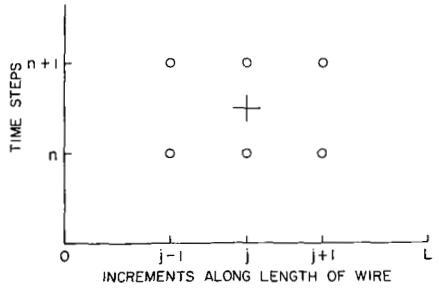

Figure 7. – Stencil for the Crank-Nicholson finite difference scheme.

In figure 7, the centering point for the difference equations is indicated by +. The circles in the stencil represent the mesh points where the temperature values are determined.

The unknown temperature $T_{j,n+1/2}$ required to calculate $b_{j,n+1/2}$ in equation (22) is initially predicted to be equal to $T_{j,n}$ and the solution $T_{j,n+1}$ is obtained as described above. The value $T_{j,n+1/2}$ is corrected by averaging $T_{j,n}$ and $T_{j,n+1}$, and a new iterated solution $T_{j,n+1}$ is found. This process of iterating over a time step is continued until the relative error of two successive solutions is within a prescribed tolerance.

The restriction on the time increment (ref. 7) for convergence and stability of the Crank-Nicholson finite difference scheme is

$$\Delta t \leq \frac{2(\Delta x)^2}{2a(x) + (\Delta x)^2 b(x, t, \bar{T}_S)}$$

Keller (ref. 7) also shows that for a linear analog the error $e_{j,n}$ between the true solution and the approximate solution obtained using the Crank-Nicholson method has a second-order bound

$$|e_{j,n}| \leq 0[(\Delta x)^2] + 0[(\Delta t)^2]$$

The numerical method was coded in Fortran IV(G) using the IBM 360/67 at Ames Research Center.

PARAMETRIC STUDY

The computer program was used to evaluate the effects of various parameters on the response of a sensor mounted on the PAET or Viking vehicles and flown in proposed Earth and Mars trajectories (tables 1 and 2). The method was to vary the value of one parameter at a time and observe the effects on the sensor time-temperature history. The effects of (1) sensor diameter, (2) sensor length, (3) sensor thermal conductivity, (4) recovery temperature ratio, (5) solar radiation, (6) vehicle-emitted infrared radiation, and (7) time of deployment were studied.

The sensor consisted of a butt-welded chromel-alumel thermocouple wire suspended between two support posts (fig. 1). The physical appearance of the weld was that of a continuous piece of wire. The wire was 0.0127 cm (0.005 in.) in diameter, and 1.4 cm long. The chromel end of the wire was spot-welded to a chromel support post, and the alumel was welded to an alumel post. The remainder of the electrical circuit was not specifically considered, but was assumed to be standard thermocouple measuring circuit. The sensor was mounted near the outer edge of the forebody, $S/R_B = 0.985$ for PAET and 0.925 for Viking, and was oriented normal to the air flow. It was assumed to be housed inside the entry vehicle until a predetermined Mach number was reached, at which time it was deployed beyond the boundary layer.

PAET-Earth Mission

The Earth-entry computer solutions were initiated, with one exception, when the entry vehicle had slowed to a Mach number of 2. The sensor on PAET was to be deployed at this Mach number. The values assigned to the various parameters in the computer solutions are given in table 3. In addition to these, (1) recovery temperature ratios were obtained from Scadron and Warshawsky's data (ref. 4), plotted in figure 4; (2) heat-transfer coefficients were obtained from figure 5; (3) pressure coefficients, C_p were obtained from experimental data, figure 8; (4) support-post temperatures were obtained from a computer solution of freely supported posts at flow conditions corresponding to the sensor location, figure 9; and (5) surface temperatures of the vehicle forebody, which radiates to the sensor, were obtained from predictions, figure 10.

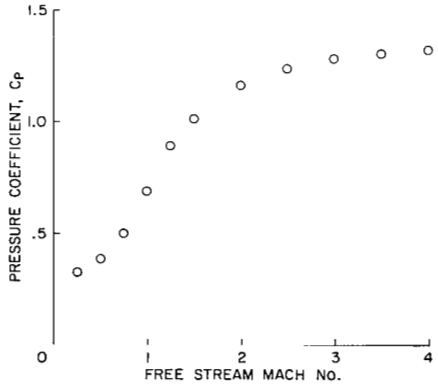

Figure 8. – Pressure coefficient versus Mach number for the PAET vehicle at zero angle of attack; sensor located at $S/R_B = 0.985$.

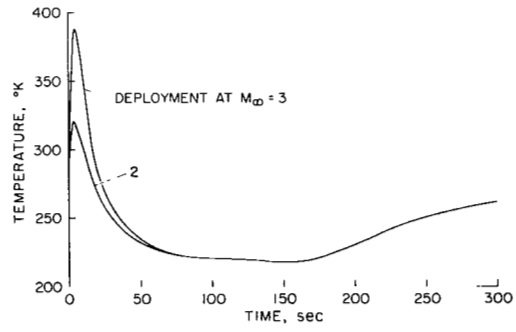

Figure 9. – Support-post temperatures for the PAET-Earth study.

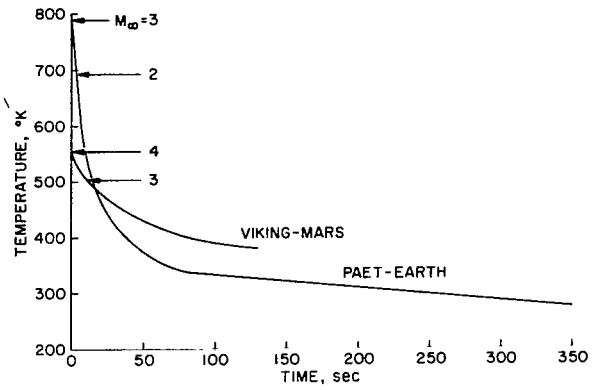

Figure 10. – Forebody temperature, near the sensor, versus time.

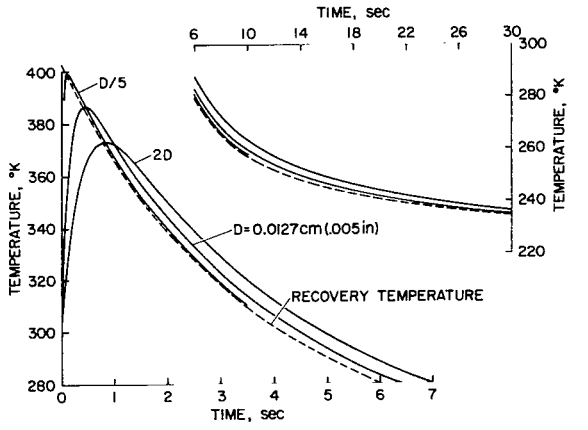

(a) Effect of sensor diameter.

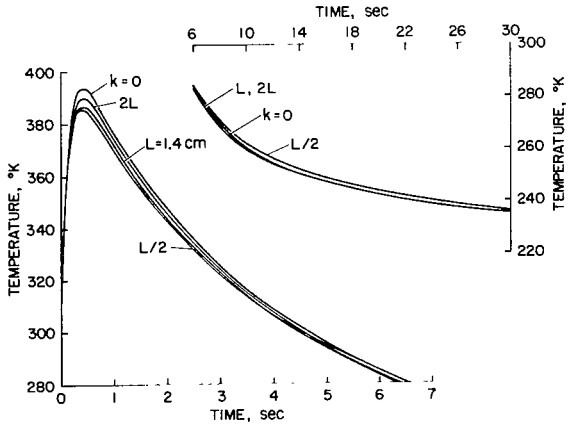

(b) Effect of sensor length and thermal conductivity.

Figure 11. – Response of sensors deployed at $M_\infty = 2$ during PAET-Earth mission.

The time response of the 0.0127-cm-dia sensor to be flown on PAET is illustrated in figure 11(a). The response curve corresponds to computer run 1 in table 3, and represents the nominally expected values of the various parameters. This figure is a plot of sensor temperature versus time, with time beginning at the instant of deployment and continuing to 30 sec. This time span is considered illustrative of the problems of measurement. In actual flight, measurements will be made over a longer time. The dashed curve represents recovery temperature, which is the temperature directly available for driving convective heat into the sensor.

The sensor temperature is seen to increase rapidly after deployment, where its initial temperature is 300° K, and in 0.4 sec reaches recovery temperature. Thereafter, however, the sensor lags this temperature because of its own thermal mass and because vehicle deceleration causes the recovery temperature to fall rapidly. At $t = 1$ sec, the difference between sensor and recovery temperatures is 6° K; at $t = 6$ sec, 3° K; and at $t = 30$ sec, less than 1° K. Thus the maximum difference occurs at about 1 sec, and thereafter continually decreases with time. The useful measurement period begins at $t = 0.4$ sec, when $M_\infty = 1.92$ and the altitude is 30.2 km.

Figure 11(a) also illustrates the effect of sensor diameter on response. The curve labeled $D/5$ is for a 0.00254-cm (0.001-in.)-dia sensor, and the one labeled $2D$ is for a 0.0254-cm (0.010-in.)-dia sensor. These correspond to computer runs 2 and 3 in table 3. The smaller sensor has a decided advantage in speed of response and overall accuracy. It reaches recovery temperature in about 0.1 sec, and thereafter its temperature difference with respect to recovery temperature is less than 1.5° K. The larger sensor has a very slow time response, requiring almost 0.8 sec to reach

recovery temperature. It has a maximum difference of 10° K, and this only slowly decreases with time. The reasons the intermediate size sensor was selected for the PAET mission are that its time response was adequate for objectives, and that it was considerably more rugged, for handling purposes, than the smaller one.

The effects of varying the length and thermal conductivity of the sensor are illustrated in figure 11(b). Three lengths of wire – corresponding to L, $L/2$, and $2L$ – and the case of zero thermal conductivity were considered. The purpose of these studies was to evaluate how closely the various lengths of wire correspond to the ideal situation of an infinitely long wire, or zero thermal conductivity. Thus, in this figure, the zero thermal conductivity case is considered ideal. At about 0.4 sec after deployment, the difference between the ideal case and the other sensors is a maximum. The maximum difference is about 8° K and depends on sensor length. The reason for these large temperature differences is that the wire rapidly responds to the high recovery temperature, but the more massive support posts do not respond so fast, with the consequent loss of heat by conduction to the support posts. Fortuitously, however, the $L/2$ sensor would fall closer to true recovery temperature for relatively early times. At later times, the temperature of the L = 1.4-cm sensor is effectively that of an infinitely long sensor wire.

The effects of solar, vehicle-emitted, and sensor-emitted radiation on the accuracy of measurement are illustrated in figure 11(c). Each radiation level was assigned a value of zero, corresponding to computer runs 7, 8, and 9 in table 3, and these were compared with the response curve for the nominally expected radiation levels (computer run 1). The responses for zero values of solar and sensor-emitted radiation were so nearly identical to those

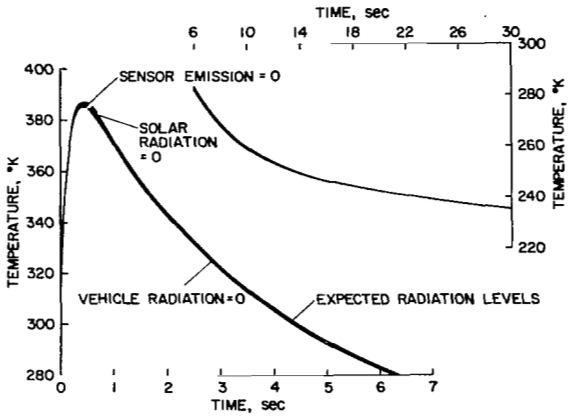

(c) Effect of solar, vehicle-emitted, and sensor-emitted radiation.

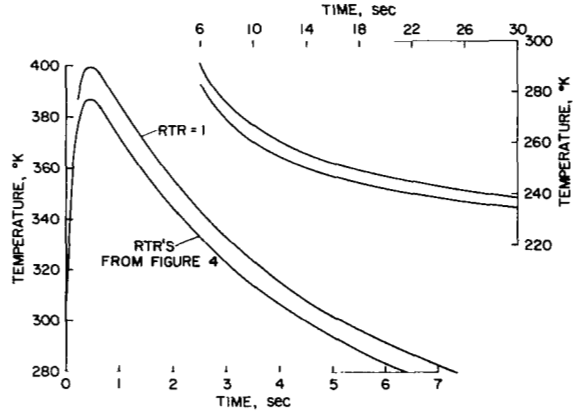

(d) Effect of recovery temperature ratio.

Figure 11. – Concluded.

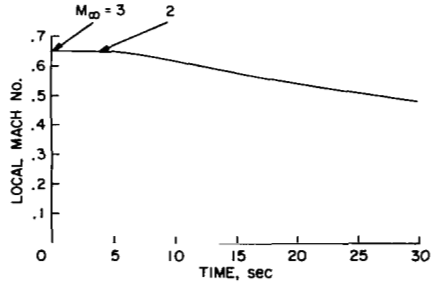

Figure 12. – Local Mach number, at sensor location, versus time; for PAET-Earth mission.

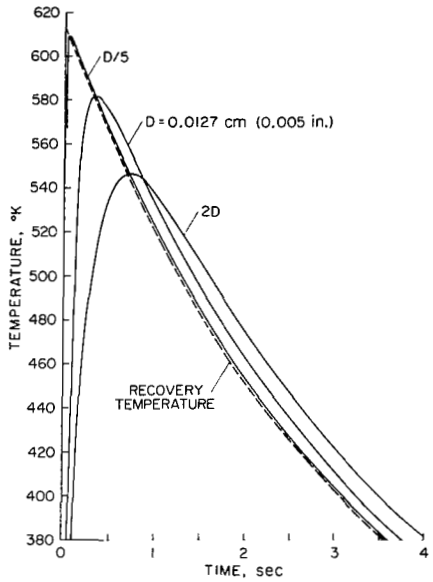

(a) Effect of sensor diameter.

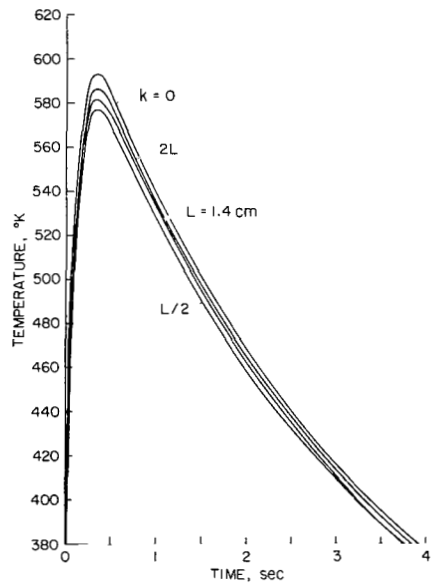

(b) Effect of sensor length and thermal conductivity.

Figure 13. – Response of sensors deployed at $M_\infty = 3$ during PAET-Earth mission.

for the nominally expected levels that for the most part these curves are shown as one. The relation of one to the other is shown slightly exploded at about 0.4 sec where the small differences start to appear (the actual total spread of the four curves at $t = 0.4$ sec was found to be only 1.6° K). The largest error was for the case of zero vehicle radiation, but even this error was less than about 1° K. It can be concluded that for the PAET mission, and deployment at Mach number 2, the influence of radiation on measurement is negligible.

Figure 11(d) illustrates the effects of varying recovery temperature ratio. The cases of $RTR = 1$ (computer run 10) were compared with those for RTR from figure 4, ref. 4 (computer run 1). The effect is quite large, amounting to the order of 10° K, and only slowly decreases with time. The reason for this behavior can be deduced from figures 4 and 12. Figure 12 shows that local Mach number (at the sensor location behind the shock) is fairly constant but does slowly decrease with time. When the free-stream Mach number is 1 or 2, the local Mach number is only about 0.65. It can be seen from figure 4, that at Mach 0.65, $RTR \sim 0.975$. Thus, the difference between the two response curves at early times after deployment amounts to about 0.025 of total temperature, or approximately 10° K. Since local Mach number decreases only slowly with time, the temperature error too will decrease only slowly. Consequently, it is important to accurately know the value of the recovery temperature ratio.

The corresponding computer runs for deployment of the sensor at Mach number 3 during the PAET-Earth mission are illustrated in figures 13(a)-(d), which have a time scale going to 4 sec after deployment. Note that the Mach number decreases to 2 at about $t = 3$ sec. These figures illustrate that error of measurement in the first 3 sec

would be twice that for the Mach 2 deployment. The basic reason is that total and recovery temperatures are higher, and changing much more rapidly than at Mach number 2 (fig. 3), which influences the ability of the sensor to track the change. It can be seen that the difference between recovery temperature and sensor temperature for the 0.0127-cm wire, at a time of 1 sec, is about 12° K. For the 2*D* case, the error approaches 22° K. The influence of sensor length is more critical than before because of the increased temperature difference between the center of the sensor wire and support posts. Errors of the order 7° K result. The effects of radiation are again small, but larger than for Mach 2. The corresponding comparison of recovery temperature ratios produces an error of about 0.025 total temperature, or about 14° K. Thus the tracking ability of the sensor is degraded above Mach number 2.

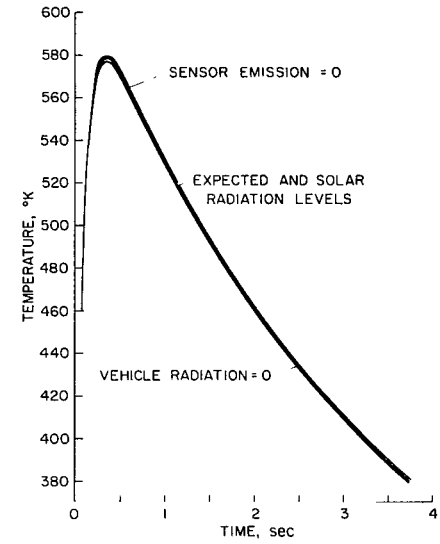

(c) Effect of solar, vehicle-emitted, and sensor-emitted radiation.

Viking-Mars Mission

An abbreviated form of the computer program was used for the Viking-Mars study. First, local Reynolds numbers at the sensor location were input to the computer (fig. 14); these numbers were used because experimental values of pressure coefficient C_p were not available, but Reynolds numbers were available from a flow-field study. Second, Mach number effects on heat-transfer coefficients (fig. 5) were neglected, and all values were computed at an arbitrary Mach number of 0.65. (It will be recalled that flow at the sensor location is always subsonic.) Third, Mach number effects on recovery temperature ratios (fig. 4) were neglected, and all ratios were arbitrarily taken as 1.0. Fourth, the temperatures of the support posts were assumed to be constant. The values assigned to the various parameters are listed in table 4; the temperature of the vehicle

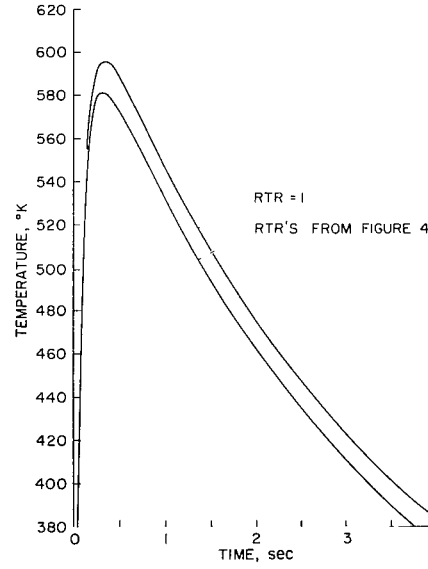

(d) Effect of recovery temperature ratio.

Figure 13. – Concluded.

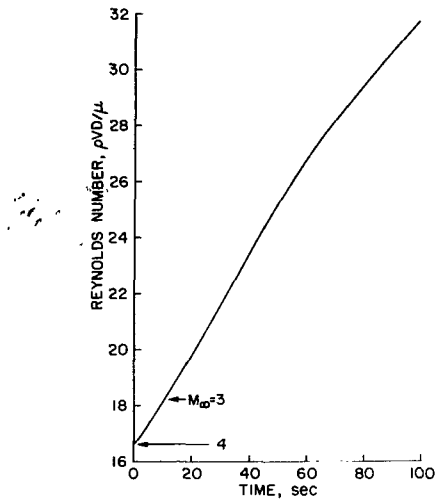

Figure 14. – Reynolds number versus time, at sensor location for Viking-Mars mission.

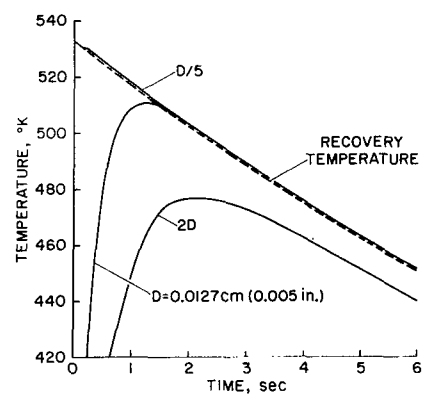

(a) Effect of sensor diameter.

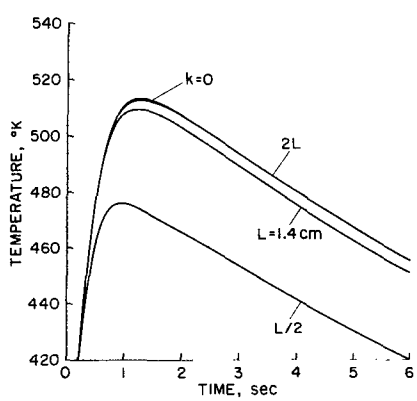

(b) Effect of sensor length and thermal conductivity.

Figure 15. – Response of sensors deployed at $M_\infty = 3$ during Viking-Mars mission.

forebody, which radiates to the sensor, is illustrated in figure 10. The sensor Reynolds numbers, local Mach number, heat-shield temperatures, and other parameters of the flow for these calculations were provided by Mr. H. C. Norman of Martin Marietta Corporation from results obtained with a flow-field computer program.

The results of the parametric study are shown in figures 15(a)-(c) for deployment at Mach number 3. A 6-sec time span was selected as illustrative of the measurement problems. The response of a PAET sensor deployed during the Viking-Mars mission, is shown in figure 15(a); $D = 0.0127$ cm. It reaches the recovery temperature in about 1.5 sec and thereafter tracks it quite well, differing by only about 1° K. Conduction effects for the selected support-post temperature of 300° K are just sufficient to counterbalance the lag in the sensor temperature. The response of sensors having $D/5$ and $2D$ diameters is also shown. The $D/5$ sensor responds in less than 0.1 sec and thereafter tracks recovery temperature within 1° K. The $2D$ sensor, however, responds very slowly and after 3 sec has errors of the order of 12° K.

Figure 15(b) shows that the sensor selected for the PAET mission is not quite long enough to eliminate conduction effects for the Viking-Mars mission; if the sensor were shortened by a factor of 2, temperature errors of the order 45° K would result. Because of conduction effects, the sensor temperature will be influenced by the specific values of support-post temperatures.

The effect of radiation on measurement accuracy is shown in figure 15(c). Solar radiation has nominally no effect due to the long distance of Mars from the Sun. Sensor self-emission and vehicle forebody

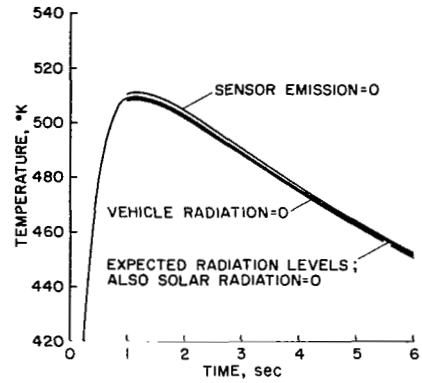

(c) Effect of solar, vehicle-emitted, and sensor-emitted radiation.

Figure 15. – Concluded.

radiation each produce errors of the order 1° K, and in opposite directions, so these effects tend to cancel one another.

Deployment at Mach number 4 is illustrated in figures 16(a)-(c). The PAET sensor and the $D/5$ diameter sensor track recovery temperature quite well, but the $2D$ sensor has errors of the order 16° K. The effect of sensor length is very prominent, and the $L/2$ sensor would produce errors of the order 60° K. Figure 16(c) shows that the effect of sensor self-emission is about 4° K.

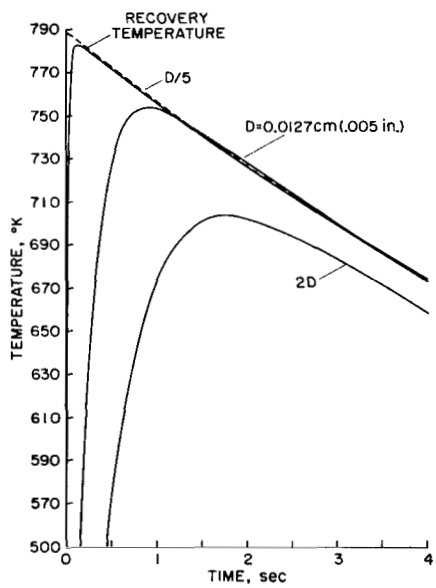

(a) Effect of sensor diameter.

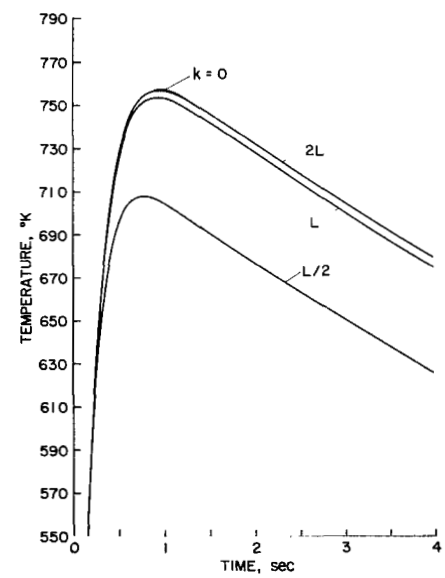

(b) Effect of sensor length and thermal conductivity.

Figure 16. – Response of sensors deployed at $M_\infty = 4$ during Viking-Mars mission.

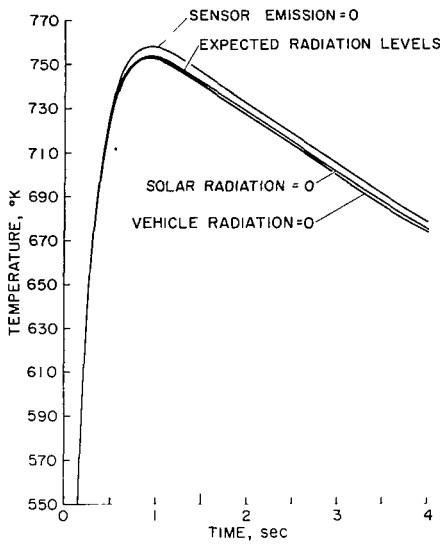

(c) Effect of solar, vehicle-emitted, and sensor-emitted radiation.

Figure 16. – Concluded.

CONCLUSIONS

An analytical study, such as the one described here, must be conducted to define the behavior and evaluate the accuracy of an atmospheric recovery-temperature sensor to be used for specific atmospheric-measurement missions. The following mission-specific factors, shown to influence the sensor design and response were included in the analysis: the relation of free-stream conditions to local Mach and Reynolds numbers at the sensor location, the heat-transfer characteristics between the sensor and the atmosphere, and extraneous heat sources such as conduction and radiation. The computer program developed for this study should be valuable for analyzing the behavior of sensors for future missions.

For the sensor selected to be flown on PAET and deployed at Mach number 2, the potential source of greatest error is an inaccurate knowledge of the recovery temperature ratio. The effects of radiation are negligible, and the sensor was designed to minimize conduction effects. For deployment at a higher Mach number (3), the sensor does not track recovery temperature as well because the temperature is higher and changes more rapidly with time. At these higher temperatures, errors in the recovery temperature ratio also produce larger errors in the deduced ambient temperature. Deployment at Mach number 3 approximately doubles the measurement error (during the increased time of measurement).

If a sensor similar to that designed for PAET, but having only half the wire length, were used for the Viking-Mars mission, the resulting errors due just to conduction effects would be of the

order 45° to 60° K. Thus, one cannot assume that a sensor proved adequate for one mission will be adequate for another.

Ames Research Center
National Aeronautics and Space Administration
Moffett Field, California 94035, April 10, 1972

REFERENCES

1. Ames Research Staff: Equations, Tables, and Charts for Compressible Flow. NACA Rep. 1135, 1953.

2. Baldwin, L. V.; Sanborn, V. A.; and Laurence, J. V.: Heat Transfer From Yawed Cylinders in Continuum, Slip and Free Molecule Air Flows. J. Heat Transfer, May 1966, pp. 77-86.

3. Simmons, F. S.: Recovery Corrections for Butt-Welded, Straight-Wire Thermocouples in High-Velocity, High-Temperature Gas Streams. NACA RM E54G22a, 1954.

4. Scandron, M. D.; and Warshawsky, I.: Experimental Determination of Time Constants and Nusselt Numbers for Bare-Wire Thermocouples in High Velocity Air Streams. NACA TN 2599, 1952.

5. Hamilton, D. C.; and Morgan, W. R.: Radiant-Interchange Configuration Factors. NACA TN 2836, 1952.

6. Jakob, M.: *Heat Transfer.* Vol. 1, Wiley, New York, 1959, p. 213.

7. Keller, H. B.: The Numerical Solution of Parabolic Partial Differential Equations. *Mathematical Methods for Digital Computers,* edited by A. Ralston and H. S. Wilf, Wiley, New York, 1960.

8. Washspress, E. L.: The Numerical Solution of Boundary Value Problems. *Mathematical Methods for Digital Computers,* edited by A. Ralston and H. S. Wilf, Wiley, New York, 1960.

BIBLIOGRAPHY

Carnahan, B.; Luther, H.A.; and Wilkes, J.O.: *Applied Numerical Methods,* Wiley, New York, 1969.

Isaacson, E.; and Keller, H.B.: *Analysis of Numerical Methods,* Wiley, New York, 1966.

Von Rosenberg, D.U.: *Methods for the Numerical Solution of Partial Differential Equations,* American Elsevier, New York, 1969.

TABLE 1 – TRAJECTORY AND PLANETARY DATA FOR PAET-EARTH MISSION

Time, sec	Altitude, km	Ambient temperature, °K	Ambient pressure, N/m^2	Ambient density, kg/m^3	Mach number	Total temperature, °K	Ratio of specific heats
0	31.6	228	942	0.0144	3.00	639	1.4
2.5	30.6	227	1100	.0169	2.17	441	
5	29.8	226	1241	.0191	1.66	351	
10	28.5	225	1497	.0232	1.10	280	
20	26.5	223	2017	.0315	.769	249	
30	24.7	221	2668	.0420	.649	240	
40	23.0	220	3475	.0551	.569	234	
50	21.4	218	4429	.0708	.505	229	
100	15.7	217	10914	.175	.309	221	
150	11.8	217	20035	.322	.225	219	
200	8.82	231	31634	.477	.178	232	
250	6.31	247	45267	.638	.149	248	
300	4.11	261	60806	.810	.128	262	
350	2.14	274	78151	.993	.113	275	
400	.347	286	97225	1.18	.101	286	
410	.007	288	101242	1.22	.099	288	

TABLE 2 – TRAJECTORY[1] AND PLANETARY DATA FOR VIKING-MARS MISSION

Time, sec	Altitude, km	Ambient temperature, °K	Ambient pressure, N/m^2	Ambient density, kg/m^3	Mach number	Total temperature, °K	Ratio of specific heats
0	23.8	197	113	0.00280	3.98	790	1.38
5	22.8	198	125	.00308	3.47	651	1.38
10	21.7	199	136	.00334	3.05	550	1.38
20	19.8	200	163	.00397	2.39	419	1.38
30	17.9	202	193	.00465	1.93	345	1.38
40	16.1	204	225	.00537	1.60	302	1.38
50	14.4	206	265	.00626	1.35	275	1.37
100	5.4	213	572	.0131	.85	242	1.37
130	0	230	905	.0190	.72	252	1.36

[1] Ballistic entry with entry velocity of 4,570 m/sec (15,200 ft/sec) ballistic coefficient of 47 kg/m^2 (0.3 $slug/ft^2$), and an entry path angle 16° below the horizontal.

TABLE 3 – VALUES OF PARAMETERS USED IN COMPUTER PROGRAM FOR PAET-EARTH STUDY

Computer run number	1	2	3	4	5	6	7	8	9	10
Sensor										
Diameter, cm	0.0127	$D/5$	$2D$	0.0127						
Length, cm	1.4			$L/2$	$2L$	1.4				
Emittance	0.14								0	0.14
Absorptance for sunlight	0.40						0	0.40		
Absorptance for planet radiation	0.14									
Absorptance for vehicle radiation	0.20							0	0.20	
View factor for sunlight	$1/\pi$									
View factor for planet radiation	0.50									
View factor for vehicle radiation	0.50									
Specific heat, J/kg°K	460									
Density, kg/m^3	8666					0				
Thermal conductivity, chromel, W/m°K	19.0					0	19.0			
Thermal conductivity, alumel, W/m°K	29.4						29.4			
Support post temperature	See fig. 9									
Recovery temperature ratio	See fig. 4									1.0
Planet										
Temperature, °K	273									
Distance from Sun, AU	1.0									

TABLE 4 – VALUES OF PARAMETERS USED IN COMPUTER PROGRAM FOR VIKING-MARS STUDY

Computer run number	1	2	3	4	5	6	7	8	9
Sensor									
Diameter, cm	0.0127	$D/5$	$2D$	0.0127					
Length, cm	1.4			$L/2$	$2L$	1.4			
Emittance	0.14								0
Absorptance for sunlight	0.40						0	0.40	
Absorptance for planet radiation	0.14								
Absorptance for vehicle radiation	0.20							0	0.20
View factor for sunlight	$1/\pi$								
View factor for planet radiation	0.50								
View factor for vehicle radiation	0.50								
Specific heat, J/kg °K	460								
Density, kg/m^3	8666								
Thermal conductivity, chromel, W/m°	19.0					0	19.0		
Thermal conductivity, alumel, W/m °K	29.4					0	29.4		
Support post temperature, °K	300								
Recovery temperature ratio	1.0								
Planet									
Temperature, °K	280								
Distance from Sun, AU	1.52								

NASA-Langley, 1972 —— 14 A-4412

"The aeronautical and space activities of the United States shall be conducted so as to contribute . . . to the expansion of human knowledge of phenomena in the atmosphere and space. The Administration shall provide for the widest practicable and appropriate dissemination of information concerning its activities and the results thereof."

—NATIONAL AERONAUTICS AND SPACE ACT OF 1958

NASA SCIENTIFIC AND TECHNICAL PUBLICATIONS

TECHNICAL REPORTS: Scientific and technical information considered important, complete, and a lasting contribution to existing knowledge.

TECHNICAL NOTES: Information less broad in scope but nevertheless of importance as a contribution to existing knowledge.

TECHNICAL MEMORANDUMS: Information receiving limited distribution because of preliminary data, security classification, or other reasons.

CONTRACTOR REPORTS: Scientific and technical information generated under a NASA contract or grant and considered an important contribution to existing knowledge.

TECHNICAL TRANSLATIONS: Information published in a foreign language considered to merit NASA distribution in English.

SPECIAL PUBLICATIONS: Information derived from or of value to NASA activities. Publications include conference proceedings, monographs, data compilations, handbooks, sourcebooks, and special bibliographies.

TECHNOLOGY UTILIZATION PUBLICATIONS: Information on technology used by NASA that may be of particular interest in commercial and other non-aerospace applications. Publications include Tech Briefs, Technology Utilization Reports and Technology Surveys.

Details on the availability of these publications may be obtained from:

SCIENTIFIC AND TECHNICAL INFORMATION OFFICE

NATIONAL AERONAUTICS AND SPACE ADMINISTRATION

Washington, D.C. 20546